Extending the self-assembly of coiled-coil hybrids

Robson, M.H.

NONCOVALENT TRIBLOCK COPOLYMERS BASED ON A COILED-COIL PEPTIDE MOTIF

The formation of a noncovalent triblock copolymer based on a coiled-coil peptide motif is demonstrated in solution. A specific peptide pair (E and K) able to assemble into heterocoiled coils was chosen as the middle block of the polymer and conjugated to poly(ethylene glycol) (PEG) and polystyrene (PS) as the outer blocks. Mixing equimolar amounts of the polymer-peptide block copolymers PS-E and K-PEG resulted in the formation of coiled-coil complexes between the peptides and subsequently in the formation of the amphiphilic triblock copolymer PS-E/K-PEG. Aqueous self-assembly of the separate peptides (E and K), the block copolymers (PS-E and K-PEG), and equimolar mixtures thereof was studied by circular dichroism, dynamic light scattering, and cryogenic transmission electron microscopy. It was found that the noncovalent PS-E/K-PEG copolymer assembled into rod-like micelles, while in all other cases, spherical micelles were observed. Temperature-dependent studies revealed the reversible nature of the coiled-coil complex and the influence of this on the morphology of the aggregate. A possible mechanism for these transitions based on the interfacial free energy and the free energy of the hydrophobic blocks is discussed. The self-assembly of the polymer-peptide conjugates is compared to that of polystyrene-*b*-poly(ethylene glycol), emphasizing the importance of the coiled-coil peptide block in determining micellar structure and dynamic behavior.

INTRODUCTION

Amphiphilic block copolymers derived from synthetic monomers can self-assemble into well-defined assemblies, such as micelles, vesicles, and networks.[1] Researchers are increasingly focusing on the use of peptide- and protein-based segments as replacements for one of the traditional polymer blocks because polymers based on amino acids have the ability to adopt structures with precisely defined shapes and spatial distributions of functionality, making them attractive building blocks for the bottom-up approach to the production of nanostructures.[2] It has been demonstrated that the degree of control over the organization of polymer assemblies can be increased not only by using well-defined building blocks but also, more recently, by utilizing noncovalent bonding motifs within the block copolymer.[3] On the basis of this principle, supramolecular polymers have been

constructed using metal-ligand coordination, hydrogen bonding, and π-π interactions.[4] In this manner, it is possible to obtain dynamic systems based on supramolecular interactions in which the association constants are controlled by external parameters such as temperature, solvent, and concentration. Although dynamic reversible assemblies based on noncovalent interactions are ubiquitously present in nature,[5] examples of synthetic assemblies in aqueous systems bearing these properties are rare.[6] As an example from nature, several specific peptide sequences have been demonstrated to generate precisely defined noncovalent complexes. A prominent motif in nature is the coiled-coil assembly of helical peptides, which is found in up to 10% of eukaryotic proteins,[7] including transcription factors, motor proteins, chaperone proteins, and viral fusion proteins. Coiled coils are formed through the coiling of two or more α-helical peptides around each other in a very specific manner that produces a stable complex in aqueous solution.[8] The oligomerization state (2-7 peptides[9]), size (~ 2 nm[10] to 200 nm[11]), direction of binding (parallel[12] or antiparallel[13]), choice of homo- [14] or heterobinding,[15] and stability[14] can be controlled by careful selection of the amino acids (natural or synthetic[16]) that constitute the peptides. The noncovalent association of these peptides is sensitive to changes in external parameters (e.g., pH, temperature, ionic strength, and solvent), which affect both the electrostatic and hydrophobic interactions, and this responsiveness permits control over the association state of the peptides.[17] As a result, incorporation of coiled-coil forming peptides into hybrid macromolecules is a vital field of research, as it allows enhanced control over nano-, micro-, and macrostructure.

Coiled coils have previously been applied to connect proteins[18] and hydrophilic polymers,[19] forming hydrogels. In these constructs, coiled-coil motifs flank a water-soluble protein or polymer segment, and the coiled-coil interaction creates a randomly connected network. This peptide motif has also been employed to reassemble complementary protein segments, restoring the original function of the proteins.[20] Aggregation of gold particles decorated with coiled-coil-forming peptides has been accomplished as a result of the interparticle peptide-peptide interaction.[21] Coiled-coil-forming peptides that associate in a staggered way, such that each peptide is involved in two coiled-coil interactions simultaneously, have been used to create fibers [22] having lengths as great as hundreds of micrometers.[23] Fractal structures have also been observed in solutions of coiled coils cross-linked through cysteine residues.[24] In all of these examples, assembly of the nanostructures is driven solely by the coiled-coil peptide interaction. The coiled-coil motif has also been connected to a poly(ethylene glycol) (PEG) block.[25] The PEG wraps around the peptide without inhibiting the formation of coiled-coil complexes. These hydrophilic hybrids do not exhibit any higher-order assembly. In this work, the complexity in this field is extended by incorporating a hydrophobic block and a hydrophilic block into peptide-polymer hybrids, thereby demonstrating hierarchical self-assembly of “smart” nanostructures in which both coiled-coil formation and, for the first time, hydrophobic-block-induced aggregation into larger assemblies coexist and influence the final structures that form.

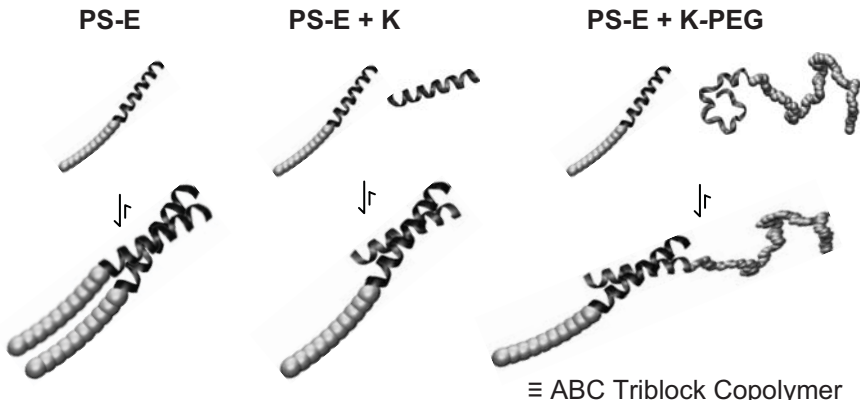

Figure 1. Schematic representation of the hierarchical self-assembly of the hybrids PS-E and K-PEG containing complementary peptide blocks. PS is polystyrene, PEG is poly(ethylene glycol), and E and K are peptides.

Using as a basis an α-helical coiled-coil pair (E and K) that exclusively forms parallel heterodimers,[8,26] a pair of polymer-peptide block copolymers were designed, PS-E and K-PEG (Table 1), containing polystyrene (PS) and PEG blocks, respectively, as the synthetic polymers. These molecules undergo two levels of self-assembly upon dispersion in solution: the specific association of the peptide pair leads to the formation of the new amphiphilic hybrid ABC triblock copolymer PS-E/K-PEG (Figure 1), which subsequently self-assembles into rod-like micelles. Reversible dissociation of the coiled coil was induced by temperature control, resulting in the transition of the rod-like micelles into spherical micelles. The self-assembly behavior of the peptides and the block copolymer PS-PEG was also studied for comparison. These experiments were used to emphasize the influence of the coiled-coil peptide interaction on the formation of the PS-E/K-PEG complex and subsequent formation of the rod-like micelles as well as on the ability to change the morphology of the self-assembled nanostructures.

RESULTS AND DISCUSSION

Peptide and Polymer-b-Peptide Design

The objective was to design a dynamic noncovalent triblock copolymer able to assemble into well-defined aggregates in aqueous solution. In order to create an amphiphile, it was chosen to design one of the outer blocks to be hydrophobic and the other to be hydrophilic in nature. The coiled-coil motif was chosen to control the self-assembly process and was used as the middle block in order to bring the hydrophobic and hydrophilic blocks together to give the noncovalent triblock copolymer PS-E/K-PEG. The pair of 22-mer peptides E and K was selected on the basis of the well-defined shape, size, and stability of the peptide parallel heterodimer.[8,26] Typically, α-helical peptides able to form a coiled-coil motif consist of a heptad repeat sequence (abcdefg).[27] This peptide pair, whose members each contain only three heptad repeats, is amongst the shortest that exclusively forms stable heterodimers. The peptides E and K chosen for this study are designed to favor heterodimer formation over homodimerization because of the presence of oppositely charged residues at the e and g positions.[27] In this way, potential homodimer formation is destabilized whereas the E/K heterodimer is stabilized through electrostatic interactions. The charged residues at position f have charges opposite those at positions e and g in order to increase the solubility and reduce the net charges of the peptides. The hydrophobic core (positions a and d) contains isoleucine and leucine, which pack together well in a "knobs-into-holes" fashion.[28] Alanine is present in the remaining two positions in order to increase the helical propensity of the peptides (Table 1). Since the peptides E and K are designed to form parallel dimers, the polymers must be conjugated at opposite ends of the peptides if formation of a coiled-coil complex is to result in a linear ABC triblock copolymer. Therefore, peptide E was conjugated at the N-terminus with hydrophobic monocarboxy terminated polystyrene to give the block copolymer PS-E, which had a polydispersity index (PDI) of 1.01. In order to form a hydrophilic corona upon self-assembly, peptide K was conjugated at the C-terminus to poly(ethylene glycol), resulting in K-PEG (PDI = 1.05). To show the importance of the coiled-coil motif on the self-assembly process, PS-PEG (PDI = 1.03), which has block lengths similar to those in the hybrid PS-E/K-PEG complex, was synthesized for comparison. All of the peptides and polymer-peptide hybrids were prepared by solid-phase peptide synthesis protocols using standard Fmoc chemistry. Sieber amide resins were used for the syntheses of E, K, and PS-E. In the synthesis of PS-E, monocarboxy-terminated polystyrene (PSCOOH) with a number-average molecular weight (M_n) of 2400 g mol-1 and a PDI of 1.20 was coupled to the N-terminus of E on the resin for 5 days. For K-PEG, K was synthesized on a PAP tentagel resin that was preloaded with a PEG block (Fmoc-NH-PEG-OH, M_n = 3400 g mol^{-1}, PDI = 1.02). All of the compounds were purified using precipitation protocols and reversed-phase high-performance liquid chromatography (RP-HPLC) and then characterized using NMR spectroscopy and matrix-assisted laser desorption ionization-time-of-flight (MALDI-TOF) mass spectrometry (Figures A1-A3 in the Appendices).

Table 1. Peptide Sequences and Hybrid Compositions.

Name	Structure[a]	M_n (g/mol)[b]	PDI
K	Ac-$(KIAALKE)_3$G-NH_2	2378	-
E	Ac-G$(EIAALEK)_3$-NH_2	2380	-
K-PEG	Ac-$(KIAALKE)_3$G-PEG_{77}	5832	1.05
PS-E	PS_9-G$(EIAALEK)_3$-NH_2	3341	1.01
PS-PEG	PS_{11}-PEG_{74}	4500	1.03

[a] PEG = poly(ethylene glycol), PS = polystyrene, Ac = acetyl. The sequences are written using the one-letter amino acid code. [b] Determined by MALDI-TOF mass spectrometry.

Peptide Self-Assembly

The secondary and quaternary structures of the peptides in buffered solution were evaluated by circular dichroism (CD) spectroscopy. Peptide E adopts a predominantly random-coil conformation, while K exhibits a predominantly α-helical spectrum. Both peptides exist in the monomeric state, as indicated by the observed ellipticity ratios ($[\theta]_{222}/[\theta]_{208}$) of 0.59 and 0.74, respectively[29] (Figure 2a and Table 2). When peptides E and K were combined in an equimolar ratio, denoted E/K, a typical α-helical CD spectrum was exhibited, with minima at 208 and 222 nm (Figure 2a). The ellipticity ratio was determined to be 0.94, consistent with interacting α-helices[29] (Table 2). This clearly shows that E and K specifically interact to form a heterodimeric α-helical coiled coil. The formation of the dimeric species was confirmed by determining the molecular weights using sedimentation equilibria, revealing that separate solutions of E and K are purely monomeric while the mixture of E/K exists as dimers (Table 3).

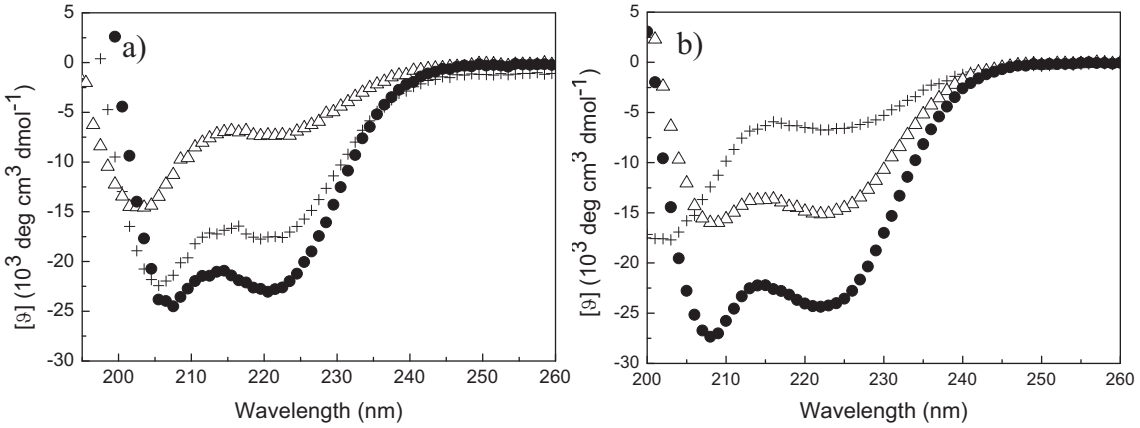

Figure 2. CD spectra of (a) E (Δ), K (+), and an equimolar mixture of E and K (●) and (b) PS-E (Δ), K-PEG (+), and an equimolar mixture of PS-E and K-PEG (●). Conditions: [total peptide] = 150-210 μM, PBS, 25 °C.

Table 2. CD Spectroscopic Data of Synthetic Peptides, Polymer-b-Peptides, and Mixtures Thereof.

Sample[a]	$[\theta]_{222}/[\theta]_{208}$		% α-helicity[b]	Coiled coil[c]
	PBS	50% TFE	PBS	
K	0.74	0.77	56	-
E	0.59	0.80	22	-
E/K	0.94	0.78	74	+
K-PEG	0.53	0.75	37	-
PS-E	0.95	0.78	48	+
E/K-PEG	0.86	0.79	37	+
PS-E/K	0.91	0.79	33	+
PS-E/K-PEG	0.89	0.77	77	+

[a] A/B refers to a mixture having equimolar concentrations of compounds A and B. [b] The % α-helicity is 100 times the ratio of the $[\theta]_{222}$ value observed in PBS to the $[\theta]_{222}$ value predicted for an α-helical peptide of n residues. The predicted α-helicity is calculated using the formula $[\theta]_{222} = -40000(1 - 4.6/n)$.[30] [c] The + sign signifies a significant decrease in the $[\theta]_{222}/[\theta]_{208}$ ratio in going from PBS to 50% TFE in PBS, indicative of the folded coiled-coil structure in PBS.[8] Conditions: [total peptide] = 150-210 μM, T = 25 °C.

Table 3. Sedimentation equilibrium data of the peptides used in this study.

name	Calculated monomeric molecular weight (g/mol)	observed molecular weight (g/mol)	oligomerization state
K	2378	2675	Monomer
E	2380	2446	Monomer
K/E	2379	4069	Dimer

Polymer-Peptide Self-Assembly

Circular Dichroism

As discussed in the Introduction, the function of the peptide blocks is to control the behavior of the synthetic polymer blocks, i.e., to assemble them into a supramolecular ABC triblock copolymer. However, the interaction between the peptides E and K can be influenced by the presence of the synthetic polymers. CD spectroscopy (Figure 2b and Table 2) showed that K-PEG adopts a random-coil secondary structure, probably due to wrapping of the PEG around the peptide.[25] A comparison of the hydrodynamic diameters (D_h) of K and K-PEG (5.1 vs. 5.4 nm) supported this interpretation. This tight packing of the PEG chain around K results in a different environment for the peptide, disturbing the hydrogen bonding that maintains the helical secondary structure in peptides. An opposite effect was observed when PS was conjugated to peptide E to form PS-E. While E adopts a random-coil conformation in solution, the spectrum of the PS-E conjugate was typical of those for interacting helices (ellipticity ratio of 0.95, 48% α-helicity). Stabilization of the α-helical structure in collagen-like peptides by hydrophobic alkyl tails has been demonstrated previously,[31] and in the present study, this observation is attributed to PS-induced aggregation (see below) that results in forced close contact of multiple E peptides and subsequent coiled-coil folding between E peptides. Mixing PS-E with K-PEG to form

PS-E/K-PEG produced increases in the ellipticity ratio and the % α-helicity (to 0.89 and 77%, respectively), indicating the formation of a coiled-coil complex similar to E/K.32 CD spectra were also recorded after the samples were diluted 1:1 (v/v) with trifluoroethanol (TFE), as TFE is known to enhance α-helicity while disrupting quaternary structures.[33] Therefore, adding TFE to monomeric peptides increases the ellipticity ratio to ~80%, while addition of TFE to coiled coils reduces this ratio to ~80%. As expected for PS-E/K-PEG, a significant decrease in the ellipticity ratio (to 0.77) was observed, which is typical of the transition from coiled coils to single helices with nearly maximum α-helicity. Combining these results shows that the ability of the peptides E and K to form heterocoiled coils is almost completely retained upon conjugation with two vastly different polymer chains. These findings imply the formation of a noncovalent ABC triblock copolymer (PS-E/K-PEG) with an amphiphilic nature.

Dynamic Light Scattering

Next, the process of self-assembly of the noncovalent PS-E/K-PEG complex into larger structures was studied using dynamic light scattering (DLS) and electron microscopy. The peptides, polymer-*b*-peptide conjugates, and mixtures thereof were dialyzed into phosphate buffered saline (PBS) starting from dimethylformamide (DMF). As expected, DLS did not show any aggregate formation for water-soluble E, K, and K-PEG or for the complexes E/K and E/K-PEG. In contrast, all of the samples containing PS assembled into defined aggregates. For PS-E, a D_h value of 16.2 $\pm$ 3.3 nm was observed (Figure 3 and Table 3). Mixing PS-E with K resulted in a small decrease in D_h (to 13.7 $\pm$ 3.2 nm). This occurred because complexation of K with E results increases the ratio of the area of the headgroup to the volume of the hydrophobic block and thus effectively decreases the packing parameter, resulting in a reduced radius for the spherical micelles.34 Combining equimolar amounts of PS-E with K-PEG increased the area of the hydrophilic headgroup of the resulting PS-E/K-PEG complex, and as a result, larger aggregates, having a D_h of 39.7 $\pm$ 11.3 nm, were observed. This large increase in micellar size was not expected on the basis of traditional packing-parameter considerations, and another model was adapted in order to explain the observations (see below).

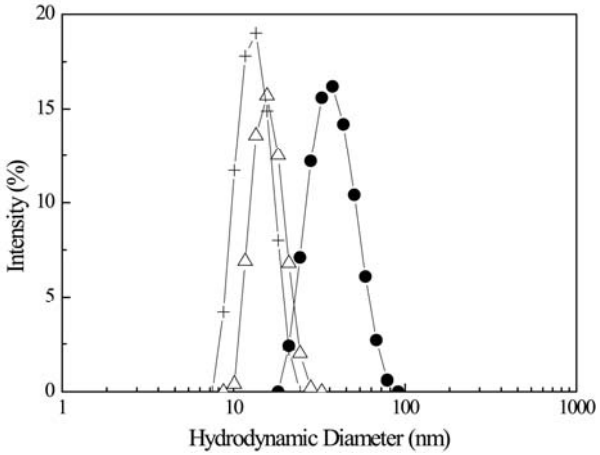

Figure 3. DLS intensity distributions for PS-E (Δ), PS-E/K (+), and a mixture of PS-E and K-PEG (●). Conditions: [total peptide] = 150-210 μM, PBS, 25 °C.

Cryogenic Transmission Electron Microscopy

Further insight into the morphologies of the assemblies was obtained by cryogenic transmission electron microscopy (cryo-TEM). These studies revealed the presence of aggregates for PS-E and the complexes PS-E/K and PS-E/K-PEG (Figure 4A-F). The micrographs showed that PS-E and PS-E/K assembled into spherical micelles with mean effective diameters (D_{eff}) of 15 $\pm$ 2 and 13 $\pm$ 3 nm, respectively (the size distributions of these micelles are presented in Figure A8 in the Appendices). In contrast, the noncovalent amphiphilic ABC triblock copolymer PS-E/K-PEG assembled into rod-like micelles with dimensions (length × width) of (42 $\pm$ 10 nm) × (8 $\pm$ 1 nm) and an average apparent aspect ratio of 5.35 Moreover, careful examination of the cryo-TEM images revealed that high electron-density regions separated by low-density regions were present along the rod. On the basis of the molecular structure of the ABC block copolymer, it is proposed that the rod-like micelles of PS-E/K-PEG are composed of a hydrophobic PS core with a corona of E/K-PEG. The high-density regions within the corona are attributed to clustering of multiple coiled-coil segments along the aggregates, while the low-density regions are attributed to hydrated PEG chains that cannot be visualized by cryo-TEM. It is therefore also proposed that the peptide clusters are separated by PEG-rich domains, as these have been shown to fold around coiled-coil-forming peptides without affecting their ability to associate.[36] Approximately 5% of the observed rods showed a lower intensity in the core of the assembly (Figure 4E and the white box in 4C), likely arising from less-efficient removal of DMF during dialysis. This results in an increased electron-density contrast between the coiled-coil clusters and the PS core, rendering the core visible. In addition, the extra solvation of the PS core most probably allows for better microphase separation of the blocks, in contrast to the majority of the micelles. The mean diameter of the core of these cylinder-like structures, as determined from the density profiles of 16 of these rods, was well-defined, with a well-defined distance between the two walls of 4.7 $\pm$ 0.5 nm, which is close to the calculated diameter of a solvated PS_9 core (4.2 nm).[37]

These results complement the DLS measurements, as demonstrated by the calculation of effective diameter distributions for the aggregates in cryo-TEM images (Table 4). Significantly, as the ellipticity ratios of PS-E/K and PS-E/K-PEG are nearly identical (Table 2), the observed morphological differences can be attributed completely to the presence of the PEG segment in the latter complex. Finally, the structural integrities of all of the micellar forms were maintained for at least 9 months when the micelles were stored at 4 °C.

In order to study the influence of the coiled-coil complex on the self-assembly behavior, PS_{11}-PEG_{74} was studied. Upon dispersion in PBS, the exclusive formation of spherical micelles was observed. Cryo-TEM revealed a polystyrene core with a mean effective diameter of 12 $\pm$ 3 nm, and DLS gave an overall hydrodynamic diameter of 20.6 $\pm$ 4.5 nm (Figures A5 and A6 in the Appendices).

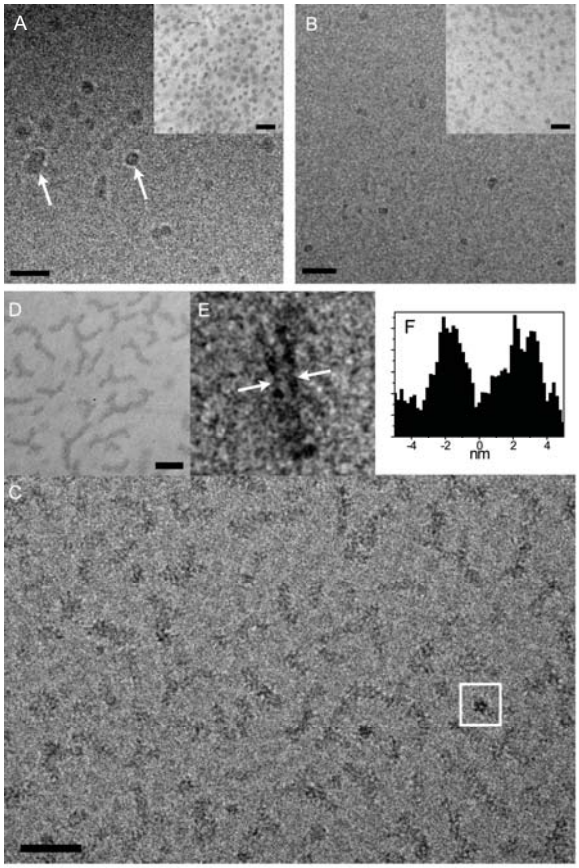

Figure 4. Cryo-TEM images of (A) PS-E, (B) PS-E/K, and (C) PS-E/ K-PEG, with 50 nm scale bars. Conditions: [total peptide] ~1500 μM, PBS. Arrows in (A) show ice particles arising from vacuum contamination. The insets in (A) and (B) and the image in (D) are phosphotungstic acid (PTA)-stained samples ([total peptide] = 150-210 μM, 50 mM phosphate, 100 mM KCl, pH 7.0, 25 °C). The micrographs in (C) and (E) show that the rods of PS-E/K-PEG are formed by small dots organized along the rod. Approximately 5% of the rods show a lower electron density in the core [viewed lengthwise in (E) and perpendicularly down the cylinder axis in the white box in (C)]. (F) The intensity profile of these rods shows a mean core diameter of 4.7 nm (representing an average calculated from 16 different profiles with a standard deviation of 0.5 nm).

Table 4. Number-Average Particle Diameters (with Standard Deviations) and Theoretical Diameters of the Aggregating Systems Investigated in This Study

Sample	Morphology	D_h (nm) [a]	D (nm) [b]	D (nm)[e]
PS-E	spherical	16.2 ± 3.3	15 ± 2	15
PS-E/K	spherical	13.7 ± 3.2	13 ± 3	13
PS-E/K-PEG	rod-like	39.7 ± 11.3	42 ± 10 x 8 ± 1[c]	length x 17
PS-E/K-PEG[f]	spherical	21.0 ± 4.4	14 ± 2[d]	18
PS-PEG	spherical	20.6 ± 4.5	12 ± 3	20

[a] Hydrodynamic diameter, as determined by DLS. The DLS data revealed a log-normal distribution of sizes. [b] Mean effective diameter, as determined from measurements of objects in TEM images. TEM size distributions are shown in Figure A8 in the Appendices. For PEG-containing samples, the dimensions obtained from TEM are smaller than those from DLS or the model, indicating that the PEG is not observed using TEM. [c] Dimensions (length × width) of the rod-like micelles. [d] PTA-stained sample. [e] Theoretical diameter, as determined using the model explained in the Appendices. [f] After annealing.

Temperature-Dependent Self-Assembly

Circular Dichroism

The temperature dependence of the assemblies was tested in order to gain insight into the dynamics and reversibility of the systems. Coiled-coil peptide complexes typically are temperature sensitive,[17] and the mixture E/K showed a melting temperature of 50 °C, as determined from the inflection point of the observed decrease in ellipticity at 222 nm (Figure 5a). The rod-like micelles composed of PS-E/K-PEG did not have a clear melting temperature, underlining the stabilizing effect of the micelles (Figure 5A). However, when the temperature reached 96 °C, the ellipticity ratio of PS-E/K-PEG mixture had decreased to less than 0.75 (Figure 5b), indicating that the peptides were no longer forming a coiled-coil complex. At this high temperature, the mixture exhibited a random-coil spectrum (Figure 5c), confirming that the specific interaction between E and K was lost, resulting in a full separation of PS-E from K-PEG (see below). When the mixture was cooled, the coiled-coil structure of PS-E/K-PEG was fully regained, as demonstrated by both the reproduction of the melting profile without hysteresis and the identical CD spectra before and after annealing (Figure 5c). These results show that the process of coiled-coil unfolding/dissociation is reversible and fast, and that the peptide structures are in equilibrium. The different shapes of the melting curves for the hybrids compared to that for E/K (Figures 5a and A9) indicates that the hybrids unfold and dissociate in a way that is atypical for coiled-coil motifs. The initial linear part of the CD melting curves corresponds to changes in helicity in the peptide complex (for example, end-fraying or unimolecular rearrangement) that occur before the onset of the cooperative unfolding and dissociation corresponding to the sigmoidal decrease in helicity seen in the E/K profile.[38] The fact that the initial linear parts of the CD melting curves for the hybrids extended from 30 °C for E/K to 70 °C for all three forms of micelle means that the PS core imparts stability with respect to cooperative folding of the peptide components by retaining them in close proximity. Although there was no clear cooperative dissociation phase for the

peptides in the micellar form, when the temperature reached 70 °C, the ellipticity ratio had decreased to a value less than that for which one can expect the coiled-coil motif to exist, indicating that the peptide complexes do not dissociate in the usual cooperative way but instead fray from one end to another or that the increasing magnitude of structural vibrations gradually dissociates the peptide complexes.[38]

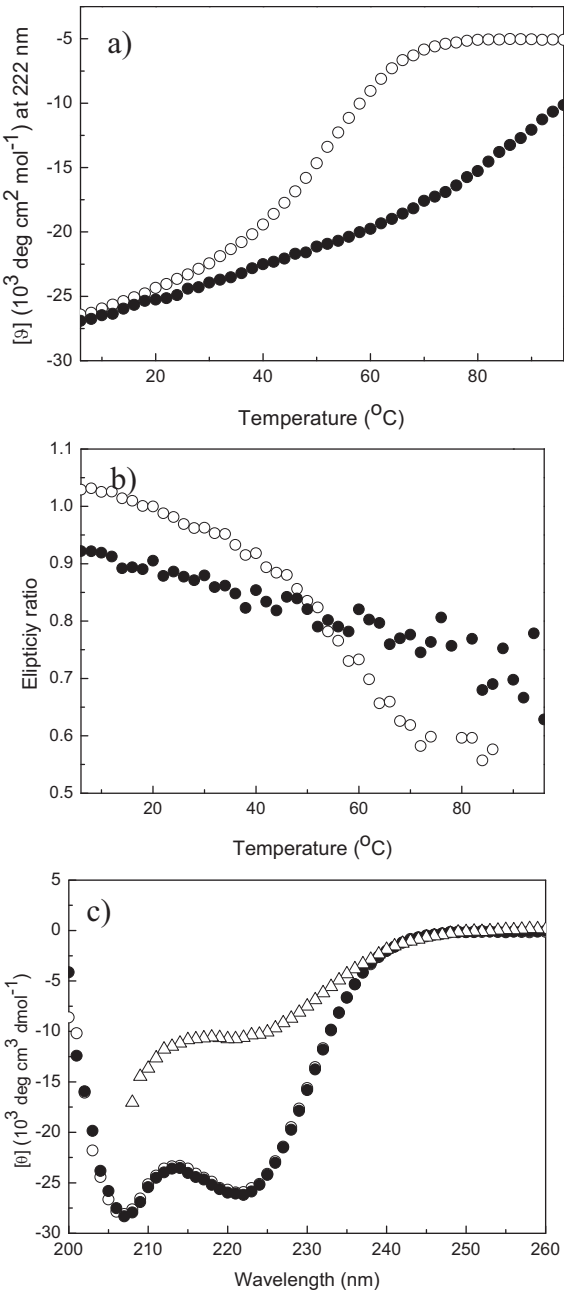

Figure 5. (a) Temperature dependence of the ellipticities ([θ] at 222 nm for E/K (○) and PS-E/K-PEG (●). (b) Temperature dependence of the ellipticity ratios for E/K (○) and PS-E/K-PEG (●). (c) CD spectra of PS-E/K-PEG at 6 °C (●), 96 °C (Δ), and after cooling back to 6 °C (○). Conditions: heating and cooling rates of 2 °C min-1, [total peptide] = 150-210 μM, PBS.

Dynamic Light Scattering

DLS of the annealed solutions of PS-E/K-PEG revealed that D_h for the rod-like micelles decreased to 21.0 $\pm$ 4.4 nm after cooling to 4 °C (Figure 6a, Table 3). Indeed, TEM revealed a conversion to spherical micelles (Figure 6b) having an average size of 14 $\pm$ 2 nm, and rod-like micelles were no longer observed. These results indicate that although the temperature-dependent assembly of the coiled-coil peptide motif is fully reversible, morphological transitions of the entire assembly are subject to more-complex kinetics.

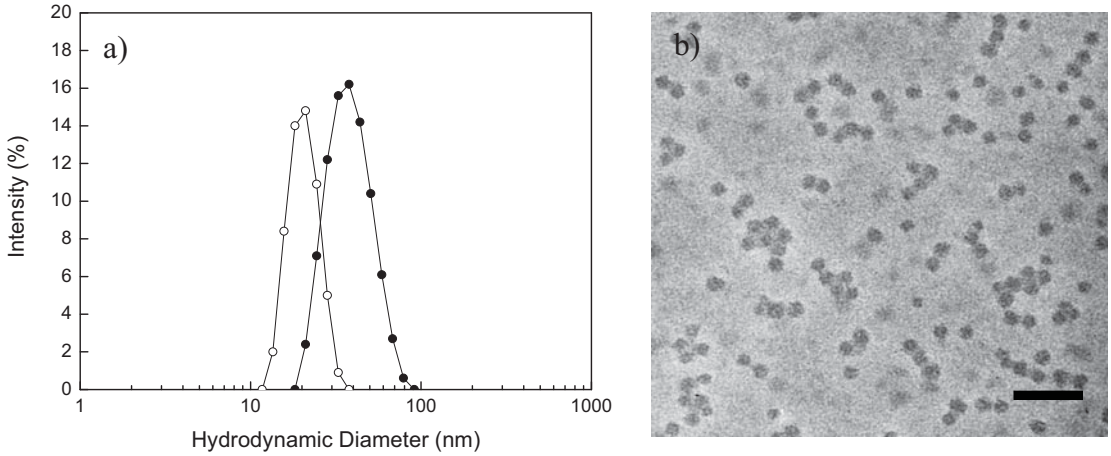

Figure 6. (a) Size distributions obtained from DLS of PS-E/K-PEG before (●) and after (○) a heating-cooling cycle. (b) PTA-stained TEM image of PS-E/K-PEG after annealing, with a scale bar of 50 nm. Conditions: [total peptide] = 270 μM, PBS, 25 °C.

A more detailed inspection of the temperature-dependent DLS data (Figure A10 in the Appendices) revealed that the rod-like micelles are stable up to ~ 45 °C. Between 45 and 75 °C, a transition of the aggregate morphology occurs, resulting in a 50% decrease in D_h. As 97% of the PS blocks have a glass transition temperature (T_g) lower than 45 °C, melting of the polystyrene core is unlikely to be the cause for this transition.[39] Temperature-dependent DLS data for the PEG homopolymer (PEG_{77}) did not reveal a significant decrease in size with increasing temperature (Figure A10), so a temperature-induced collapse of PEG chains is also unlikely to trigger the change in aggregate size. Hence, the observed size decrease must be a consequence of the temperature-dependent dissociation of the peptides (Figure 5a). In contrast, thermal cycling of PS-PEG micelles revealed the stability of these assemblies, with only a slight, reversible decrease of 2 nm in D_h (from 23 to 21 nm) upon cycling of the temperature between 4 and 90 °C (Figure A7 in the Appendices). The formation of thermally stable spherical PS-PEG micelles is in accord with the results of previous studies of the aqueous self-assembly of PS-PEG with block lengths or polystyrene weight fractions similar to those used in this study.[40]

SUMMARY AND DISCUSSION

Experimental

The experimental results have shown that the hybrids PS-E and K-PEG undergo two levels of self-assembly: the peptides interact to produce a noncovalent triblock copolymer, which then arranges into rod-like micelles. The hydrophobic PS block forms the core, which is shielded from the aqueous buffer by clusters of coiled-coil peptides around which PEG is closely folded. The dissociation of the PS-E/K-PEG complex at high temperature leads to a change in the micellar morphology, yielding spherical micelles composed of PS-E with K-PEG free in solution, i.e., the system now behaves like the PS-E sample. When the peptides are cooled, they re-coil (as seen with CD), resulting in spherical micelles coated with PEG. The high-temperature rearrangement of the rod-like micelles studded with clusters of coiled coils into spherical PS-E micelles results in homogenous dispersion of E over the surface. Hence, when K-PEG starts to re-coil with the PS-E micelles, the PEG block forms a layer outside the peptide shell. These conclusions are supported by DLS and cryo-TEM data. DLS shows that the hydrodynamic diameter of the annealed PS-E/K-PEG spherical micelles is larger than that of PS-E/K, and the difference fits with the dimensions of the PEG block used. In contrast, similar diameters were found with TEM since PEG is not visible, further confirming that PS-E/K-PEG micelles are composed of a PS core, a peptide layer, and a PEG outer layer. The micelles remain spherical upon subsequent heating and cooling cycles, indicating that these micelles are at thermodynamic equilibrium. A schematic representation of the behavior of the triblock copolymer is shown in Figure 7.

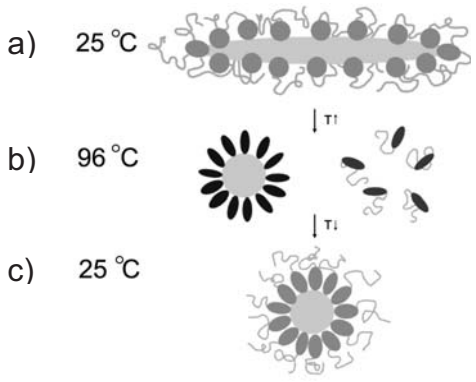

Figure 7. Idealized schematic cross-section representation of the temperature- dependent self-assembly of PS-E/K-PEG. (a) Rod-like micelles are composed of a PS core and an E/K-PEG corona. (a) Heating leads to the formation of spherical micelles with a PS core and an E corona. K-PEG is in solution. (c) When the spherical micelles are cooled, they have a PS core and an E/K-PEG corona.

The distinct difference in the self-assembly behaviors of noncovalent PS-E/K-PEG and covalent PS-PEG highlights the influence of the coiled-coil block on these processes, as

shown by the observed morphologies and temperature-dependent dynamic behaviors. In summary, PS-E/K-PEG self-assembles into dynamic rod-like micelles that are able to undergo a transition in micellar morphology, while PS-PEG organizes into static spherical micelles (see below). Thus, inclusion of the reversible noncovalent connecting block provides access to an unusual micellar morphology and encodes "smartness" into the nanostructures, allowing them to respond to environmental changes.

Model

Because direct dissolution of PS-E in buffer is not possible, micelles are produced by the gradual removal of the organic cosolvent from the amphiphile solutions. However, the presence of solvent in the core41 and the low degree of polymerization of the PS block (which has a low average T_g of 11 °C)[39] may lead to equilibrated micelles with mobile hydrophobic blocks. As a result, the micellar morphology becomes sensitive to external factors such as temperature, buffer concentration, interaction between monomers, and so on. The dimensions of the PS-PEG, PS-E, and PS-E/K micelles, as measured by DLS and TEM at temperatures above the T_g of the PS part, are in accordance with those of micelles having a disordered polystyrene core surrounded by a PEG or coiled-coil peptide shell. The packing parameters of PS-PEG, PS-E, and PS-E/K micelles predict the formation of micelles with spherical morphology. PS-E/K self-assembles into slightly smaller micelles than PS-E does, as the larger size of the hydrophilic block causes greater curvature in the self-assembled nanostructures and, in addition, E/K charge neutralization reduces stretching of the PS core. For the PS-E/K-PEG complex, a spherical micellar morphology for the thermodynamically favored structures is *expected* on the basis of the simple packing parameter model, as the ratio of the hydrophilic and hydrophobic block lengths increases.[34] However, for this complex, the observed morphology formed during dialysis is the rod-like structure. The packing parameter was originally designed to predict the morphology and size of nanostructures formed from lipids.[34] However, this approach has proven to be ill-suited for block copolymers like the ones considered here, as it cannot accommodate headgroup complexity such as flexibility and dynamic behavior. To qualitatively explain all of the observed morphologies and the transition from rod-like to spherical micelles, a theoretical model was adapted (see the Appendices) initially designed for charged, flexible diblock copolymers.[42] Currently, no simple model for determining the phase diagram of triblock copolymers with a rigid middle block exists. In view of the limitations of available models, the most practical model was adapted that can predict the different morphologies and transitions between them as well as the micellar dimensions that arise from the complex, noncovalent hybrids studied in this work. In order to treat the PS-E/K-PEG triblock copolymer as a diblock one, E/K-PEG was considered to be a single block. It was also assumed that the excess of salt present in the buffer neutralizes the charges of the E, K, and E/K blocks and that polymers follow the statistics of flexible neutral chains. The size of the PS core and the overall size of the micelle are established from the interplay between the free energy of the hydrophilic block (E, E/K, or E/K-PEG)

and the interfacial energy between the core and corona. For PS-PEG, PS-E, and PS-E/K complexes, the free energy of the hydrophilic group comprises the free energies of the PEG or peptide conformations and of short-range interactions between molecules. All of the spherical morphologies observed in this study are predicted by this model. PS-E and PS-E/K complexes are either in the region of spherical micelles or in the region of degenerate structures where rod-like micelles, spherical micelles, and lamella have the same free energy. Only spheres are observed because the translational entropy favors the formation of smaller objects. For comparison, PS-PEG is in a region where micelles can only be spherical. The model predicts that increasing the length of the water soluble block (through complexation of PS-E with K-PEG) leads exclusively to rod-like morphology. This is due to the low free energy of the short-range interactions between monomers per hydrophilic E/K-PEG block. This means that the PEG chains are more compact than those in PS-PEG. Temperature annealing of the rod-like complex transforms the structure into degenerate spheres. This is possible because at high temperature, the E/K complex dissociates and K-PEG leaves the micelle. The reduced amount of organic solvent in the PS core decreases the conformational entropy of PS and increases the interfacial energy. Therefore, the PS-E rearranges into degenerate spheres with a tightly packed polystyrene core. When the system is cooled, K-PEG re-coils with the PS-E micelles, but because the polystyrene core is now locked in a frozen equilibrium (tightly packed), the PS molecules are unable to rearrange into the rod-like structure upon condensation of K-PEG onto the spherical PS-E micelles or with further temperature annealing. As summarized in Table 3, the model correctly predicts the form of PS-PEG, PS-E, PS-E/K, and PS-E/K-PEG micelles and includes the transition of PS-E/K-PEG from rod-like to spherical micelles upon annealing. The micellar diameters estimated by this model are in surprisingly close agreement with the experimental results. However, the model overestimates the diameter of the rod-like micelles, indicating that it requires further tuning in order to account for the complexity of the triblock copolymer and the end-capping energy.

CONCLUSIONS

This work represents the first account of a noncovalent triblock copolymer composed of hydrophobic and hydrophilic polymers united via a peptide complex. The hierarchical self-assembly in solution of two complementary polymer-*b*-peptides (PS-E and K-PEG) utilizes the coiled-coil-forming propensities of the peptides, resulting in the formation of an amphiphilic triblock copolymer (PS-E/K-PEG) able to assemble into rod-like micelles. The dynamic nature of these micelles was shown by annealing of the amphiphile above the coiled-coil transition temperature. The release of the hydrophilic hybrid led to a transformation to spherical micelles that persisted upon re-coiling of the peptides, demonstrating the reversibility of the noncovalent block linker. As the macromolecular entities that are connected to the peptides are open to choice and additional methods for influencing the peptidic interaction exist, this peptide motif is a promising building block for the bottom-up approach to the formation of “smart” block copolymer structures in aqueous solutions.

EXPERIMENTAL SECTION

Materials and Methods

Materials

Fmoc-protected amino acids were purchased from Novabiochem. Tentagel PAP resin was purchased from Rapp Polymere. Monocarboxy terminated polystyrene was purchased from Polymer Source Inc.. All other reagents and solvents were obtained at the highest purity available from Sigma-Aldrich or BioSolve Ltd. and used without further purification. Phosphate buffered saline, PBS: 30 mM $K_2HPO_4.3H_2O$, 19 mM KH_2PO_4, 100 mM KCl, pH 7.0.

General Methods

HPLC was performed with a Shimadzu HPLC system with two LC-8A pumps, and an SPD-10AVP UV-VIS detector. Sample elution was monitored by UV detection at 214 nm and 256 nm. Samples were eluted with a linear gradient from A to B, A being 0.1% (v/v) TFA in water, and B acetonitrile. Purification of the peptides and hybrids was performed on a Vydac C4 reversed phase column (214TP1022, 22 mm diameter, 250 mm length, 10.00 μM particle size) with a flow rate of 20 mL min^{-1}. For verification of sample purity a reversed phase Vydac C4 column (214TP54, 4.6 mm diameter, 250 mm length, 5.00 μM particle size) was used with a flow rate of 1 mL min^{-1}. Sample elution was additionally monitored by an light evaporative light scattering detector. PS-PEG was purified on an Alltech Alltima Silica 5u column (22 mm diameter, 250 mm length) with a flow rate of 10 mL min^{-1} and a linear gradient from A to B, A being methanol, and B dichloromethane.

MALDI-TOF mass spectra were acquired using an Applied Biosystems Voyager System 6069 MALDI-TOF spectrometer. Samples were dissolved in 1:1 (v/v) 0.1% TFA in water:acetonitrile (TA), at concentrations of ~0.3 mg mL^{-1} for K and E, ~6 mg mL^{-1} for K-PEG and PS-PEG, and ~3 mg mL^{-1} for PS-E and PEG. Solutions for spots consisted of (v/v) 1:10 sample solution: 10 mg mL^{-1} ACH in TA. For K-PEG and PS-E one part 0.1% AgTFA in THF was added to facilitate ionization, and for the PS-E solutions 10 parts of THF were added. PSCOOH was dissolved at ~ 2 mg mL^{-1} in a dithranol solution (20 mg mL^{-1} dithranol in $CHCl_3$).

^{1}H-NMR spectra were recorded on a Bruker AV-500 spectrometer and a Bruker DPX300 spectrometer using the residual proton resonance of deuterated water, acetonitrile, or chloroform for calibration.

GPC was preformed with a Shimadzu system equipped with a refractive index detector. A Polymer Laboratories column was used (3M-RESI-001-74, 7.5 mm diameter, 300 mm length) with DMF as the eluent, at 60 ºC, and a flow rate of 1 mL min^{-1}. PEG standards were used for mass calibration.

Synthesis

Solid-Phase Peptide Synthesis of K, E, K-PEG, PS-E

The peptide components of K, E, PS-E, and K-PEG were prepared using standard Fmoc chemistry on an Applied Biosystems 431A automated peptide synthesizer. E, K, and the peptide component of PS-E were synthesized on Sieber-Amide resin, while the peptide section of K-PEG was prepared on Tentagel PAP resin. HCTU was used to activate the amino acid derivatives. K, E and K-PEG were acetylated at the N-terminus. After the peptide component of PS-E was prepared, the resin was removed from the reaction vessel, swollen in 1:1 (v/v) DMF:NMP, and Fmoc deprotected. PS was coupled to the N-terminus by shaking 4 equivalents of PSCOOH M_n 2400 g mol^{-1} (PDI 1.20), 4 equivalents of HCTU, and 8 equivalents of DIPEA (predissolved in DMF) with the resin for five days. Cleavage and deprotection of the compounds was carried out using 95:2.5:2.5 (v/v) TFA:water:TIS for 1-3 hours. The cleavage mixture and three subsequent rinses of the resin with the TFA mixture were added drop-wise to cold diethylether, or cold methanol for PS-E. With K, E, and K-PEG the white precipitate was compacted with centrifugation and the supernatant removed. This was repeated three times with the addition of fresh diethylether. The pellets were dried in air or under reduced pressure. For PS-E the solution was evaporated to dryness with toluene addition 5 times throughout the evaporation. The slightly yellow material was dried under reduced pressure.

The crude products of the K, E, and PS-E syntheses were purified by RP-HPLC, with gradient elution 35% to 50% B over 20 minutes for K and E, and 50% to 100% B over 30 minutes for PS-E. K-PEG was purified by dialysis from Spectra/Por® regenerated cellulose dialysis tubing with a molecular weight cut of 3500 g mol^{-1}. After purification all compounds were lyophilized from water (or in the case of PS-E, from a water/acetonitrile mixture) to give white material with the following yields: K, E ~ 40%, K-PEG, PS-E ~ 10%. The compounds were characterized by MALDI-TOF MS (K: m/z = 2379 $[M+H]^+$, E: m/z = 2381 $[M+H]^+$), RP-HPLC, and ^{1}H-NMR. The chromatograms and spectra for PS-E and K-PEG are shown in Figures A1–A3.For each compound the purity was estimated from RP-HPLC to be greater than 95%.

Synthesis of PS-PEG

Cleavage of NH_2-PEG_{74}-OH from Tentagel PAP resin was carried out using TFA for 15 hours. The cleavage mixture and three subsequent rinses of the resin with TFA were added drop-wise to cold diethylether. The white precipitate was compacted with centrifugation and the supernatant removed. This was repeated three times with the addition of fresh diethylether. The pellets were dried under reduced pressure. Residual acid was removed by dissolving the powder in Milli-Q water and shaking with Amberlite resin IRA-410 (OH) for 5 minutes. Lyophilizing resulted in a white powder at 80% yield. MALDI-TOF MS: M_n = 3321 gmol^{-1}.

Monocarboxy terminated polystyrene was coupled to the poly(ethylene glycol) via the amine terminus by shaking 1 equivalent of PSCOOH (MALDI-TOF MS: M_n = 1286 g

mol^{-1}, FTIR (thin film from $CHCl_3$): 1706 cm^{-1} (C=O stretch)), 1.2 equivalents of PYBOP, and 2.4 equivalents of DIPEA (predissolved in DMF, 2 minutes activation, FTIR (thin film from $CHCl_3$): 1811 cm^{-1} (C=O stretch)) with 1.4 equivalents of poly(ethylene glycol) for 15 hours.

The crude product was purified by silica HPLC, with gradient elution 100% to 90% B over 30 minutes, followed by a Bio-Beads column using chloroform as the eluent. Lyophilizing resulted in PS_{11}-PEG_{74} in the form of a white powder at 13% yield. MALDI-TOF MS: M_n = 4500 g mol^{-1}. ^{1}H-NMR (300 MHz, $CDCl_3$, δ): 7.15-6.64 (bm, 53H, PS), 3.64 (s, 296H, PEG). FTIR (thin film from $CHCl_3$): 1672 cm^{-1} (C=O stretch, Amide I band). GPC (DMF): 8.2 minutes, PDI = 1.03.

Preparation of the Micellar Suspensions

The compounds were dissolved at 1 mg mL^{-1} of peptide in DMF for the preparation of the stock solution. The stock solutions were combined in 1:1 ratios. PS-PEG was dissolved at 1 mg mL^{-1} in DMF. Dialysis tubing of molecular weight cut-off of 1000 g/mol was rinsed with water, then DMF, and the samples were dialyzed against buffer (50 mM PO4, 100 mM KCl, pH 7.0) at room temperature for at least 24 hours with at least 5 changes of buffer.

The aggregation numbers of the spherical micelles of PS-E and PS-E/K are estimated to be 270 and 110 based on the aggregate sizes observed with electron microscopy and the calculated molecular/complex volume using the program ChemDraw. PS-E/K-PEG rod-like micelles are estimated to contain 640 complexes, while the spherical PS-E/K-PEG micelles are estimated to contain 230 complexes.

Characterization of Micellar Suspensions

Circular Dichroism Spectroscopy

CD spectra were obtained as detailed in the experimental section of Chapter 2.

Dynamic Light Scattering

Experimental diffusion coefficients, D, were measured at 25 °C by dynamic light scattering using a Malvern Zetasizer Nano ZS equipped with a peltier-controlled thermostatic cell holder. The laser wavelength was 633 nm and the scattering angle was 173˚. The Stokes-Einstein relationship $D = k_BT/3\pi\eta D_h$ was used to estimate the hydrodynamic radius, D_h. Here k_B is the Boltzmann constant, and η is the solvent viscosity. Temperature dependent DLS distributions were measured from 4 °C to 90 °C with parameters optimized at each temperature.

Analytical Ultracentrifugation

Apparent molecular masses were determined by sedimentation profiles using a Beckmann XL-A ultracentrifuge at 20 °C. The peptides were dissolved in 50 mM phosphate, 100 mM KCl, pH 7.0 buffer at 1.0 mg/mL. For each sample three different concentrations where

used, namely those concentrations at which the optical density (O.D.) was 0.1, 0.3 and 0.5 respectively. The absorption of each sample was first checked with an UV-VIS photospectrometer and diluted with the buffer to reach the necessary concentration. The samples where then loaded into a charcoal/epoxy 6-channel 12 mm centerpiece, equipped with quartz windows against the buffer as a reference. The samples where then loaded into the analytical ultracentrifuge and allowed to equilibrate at three different rotor speeds namely, 25000 rpm, 33000 rpm and 40000 rpm. Data were fit to a single species, with high correlation factors, R, and random residuals.

Transmission Electron Microscopy

TEM was conducted on a JEOL 1010 instrument with an accelerating voltage of 60 kV. Samples for TEM were prepared by placing a drop of each solution on carbon-coated copper grids. After ~ 10 minutes the droplet was removed from the edge of the grid. A drop of 2% PTA stain was applied and removed after 2 minutes. Negative images are shown in order to retain image quality.

Cryogenic Transmission Electron Microscopy

Samples for cryogenic TEM were concentrated by centrifuging in Centricon centrifugal filter devices MWCO 3000 g mol^{-1} at 4˚C. Sample stability was verified by DLS and TEM.

The cryogenic transmission microscopy measurements were performed on a FEI Technai 20 (type Sphera*)* TEM or on a Titan Krios (FEI). A Gatan cryo-holder operating at ~ -170 °C was used for the cryo-TEM measurements. The Technai 20 is equipped with a LaB_6 filament operating at 200kV and the images were recorded using a 1kx1k Gatan CCD camera. The Titan Krios is equipped with a field emission gun (FEG) operating at 300 kV. Images were recorded using a 2k x 2k Gatan CCD camera equipped with a post column Gatan energy filter (GIF). The sample vitrification procedure was carried out using an automated vitrification robot: a FEI Vitrobot Mark III. TEM grids, both 200 mesh carbon coated copper grids and R2/2 Quantifoil Jena grids were purchased from Aurion. Copper grids bearing lacey carbon films were home made using 200 mesh copper grids from Aurion. Grids were treated with a surface plasma treatment using a Cressington 208 carbon coater operating at 25 A for 40 seconds prior to the vitrification procedure.

REFERENCES

1. (a) Zhang, L.; Eisenberg, A. *Science* **1995**, *268*, 1728–1731. (b) Cameron, N. S.; Corbierre, M. K.; Eisenberg, A. *Can. J. Chem.* **1999**, *77*, 1311–1326.
2. (a) Vandermeulen, G. W. M.; Klok, H.-A. *Macromol. Biosci.* **2004**, *4*, 383–398. (b) Cornelissen, J. J. L. M.; Fischer, M.; Sommerdijk, N. A. J. M.; Nolte, R. J. M. *Science* **1998**, *280*, 1427–1430. (c) Kros, A.; Jesse, W.; Metselaar, G. A.; Cornelissen, J. J. L. M. *Angew. Chem., Int. Ed.* **2005**, *44*, 4349–4352. (d) Klok, H.-A. *Angew. Chem., Int. Ed.* **2002**, *41*, 1509–1513. (e) Bellomo, E. G.; Wyrsta, M. D.; Pakstis, L.; Pochan, D. J.; Deming, T. J. *Nat. Mater.* **2004**, *3*, 244–248. (f) Boerakker, M. J.; Botterhuis, N. E.; Bomans, P. H. H.; Frederik, P. M.; Meijer, E. M.; Nolte, R. J. M.; Sommerdijk, N. A. J. M. *Chem.Eur. J.* **2006**, *12*, 6071–6080. (g) Billot, J.-P.; Douy, A.; Gallot, B. *Makromol. Chem.* **1976**, *177*, 1889–1893. (h) Vriezema, D. M.; Kros, A.; De Gelder, R.; Cornelissen, J. J. L. M.; Rowan, A. E.; Nolte, R. J. M. *Macromolecules* **2004**, *37*, 4736–4739.
3. (a) Shimizu, L. S. *Polym. Int.* **2007**, *56*, 444–452. (b) Sivakova, S.; Rowan, S. J. *Chem. Soc. Rev.* **2005**, *34*, 9–21.
4. (a) Brunsveld, L.; Folmer, B. J. B.; Meijer, E. W.; Sijbesma, R. P. *Chem. Rev.* **2001**, *101*, 4071–4097, and references cited therein. (b) Xu, J.; Fogleman, E. A.; Craig, S. L. *Macromolecules* **2004**, *37*, 1863– 1870. (c) Ilhan, F.; Galow, T. H.; Gray, M.; Clavier, G.; Rotello, V. M. *J. Am. Chem. Soc.* **2000**, *122*, 5895–5896. (d) Guillet, P.; Fustin, C.- A.; Lohmeijer, B. G. G.; Schubert, U. S.; Gohy, J.-F. *Macromolecules* **2006**, *39*, 5484–5488.
5. (a) Ohlson, S.; Strandh, M.; Nilshans, H. *J. Mol. Recognit.* **1997**, *10*, 135–138. (b) Vandermerwe, P. A.; Barday, A. N. *Trends Biochem. Sci.* **1994**, *19*, 354–358.
6. Gohy, J.-F.; Lohmeijer, B. G. G.; Alexeev, A.; Wang, X. S.; Manners, I.; Winnik, M. A.; Schubert, U. S. *Chem.Eur. J.* **2004**, *10*, 4315–4323.
7. Liu, J.; Rost, B. *Protein Sci.* **2001**, *10*, 1970–1979.
8. Litowski, J. R.; Hodges, R. S. *J. Biol. Chem.* **2002**, *277*, 37272–37279.
9. Liu, J.; Deng, Y.; Cheng, C.-S.; Kallenbach, N. R.; Lu, M. *Proc. Natl. Acad. Sci. U.S.A.* **2006**, *103*, 15457–15462.
10. (a) Dong, H.; Hartgerink, J. D. *Biomacromolecules* **2006**, *7*, 691–695. (b) Burkhard, P.; Meier, M.; Lustig, A. *Protein Sci.* **2000**, *9*, 2294–2301.
11. Kohn, W. D.; Mant, C. T.; Hodges, R. S. *J. Biol. Chem.* **1997**, *272*, 2583–2586.
12. Woolfson, D. N. *Adv. Protein Chem.* **2005**, *70*, 79–112.
13. Oakley, M. G.; Hollenbeck, J. J. *Curr. Opin. Struct. Biol.* **2001**, *11*, 450–457. (b) Hadley, E. B.; Testa, O. D.; Woolfson, D. N.; Gellman, S. H. *Proc. Natl. Acad. Sci. U.S.A.* **2008**, *105*, 530–535.
14. Yu, Y. B. *Adv. Drug Delivery Rev.* **2002**, *54*, 1113–1129.
15. Acharya, A.; Ruvinov, S. B.; Gal, J.; Moll, J. R.; Vinson, C. *Biochemistry* **2002**, *41*, 14122–14131.
16. Tang, Y.; Ghirlanda, G.; Vaidehi, N.; Kua, J.; Mainz, D. T.; Goddard, W. A., III; DeGrado, W. F.; Tirrell, D. A. *Biochemistry* **2001**, *40*, 2790–2796. (b) Ryan, S. J.; Kennan, A. J. *J. Am. Chem. Soc.* **2007**, *129*, 10255–10260.
17. (a) Schnarr, N. A.; Kennan, A. J. *J. Am. Chem. Soc.* **2003**, *125*, 6364–6365. (b) Stevens, M. M.; Allen, S.; Sakata, J. K.; Davies, M. C.; Roberts, C. J.; Tendler, S. J. B.; Tirrell, D. A.; Williams, P. M. *Langmuir* **2004**, *20*, 7747–7752. (c) Naik, R. R.; Kirkpatrick, S. M.; Stone, M. O. *Biosens. Bioelectron.* **2001**, *16*, 1051–1057. (d) Wendt, H.; Leder, L.; Harma, H.; Jelesarov, I.; Baici, A.; Bosshard, H. R. *Biochemistry* **1997**, *36*, 204–213.
18. (a) Petka, W. A.; Harden, J. L.; McGrath, K. P.; Wirtz, D.; Tirrell, D. A. *Science* **1998**, *281*, 389–392. (b) Shen, W.; Zhang, K.; Kornfield, J. A.; Tirrell, D. A. *Nat. Mater.* **2006**, *5*, 153–158.
19. Wang, C.; Stewart, R. J.; Kopeček, J. *Nature* **1999**, *397*, 417–420.
20. (a) Ghosh, I.; Hamilton, A. D.; Regan, L. *J. Am. Chem. Soc.* **2000**, *122*, 5658–5659. (b) Yuzawa, S.; Mizuno, T.; Tanaka, T. *Chem.Eur. J.* **2006**, *12*, 7345–7352. (c) Chelur, D. S.; Chalfie, M. *Proc. Natl. Acad. Sci. U.S.A.* **2007**, *104*, 2283–2288.
21. Stevens, M. M.; Flynn, N. T.; Wang, C.; Tirrell, D. A.; Langer, R. *Adv. Mater.* **2004**, *16*, 915–918.
22. (a) Zhou, M.; Bentley, D.; Ghosh, I. *J. Am. Chem. Soc.* **2004**, *126*, 734–735. (b) Dublin, S. N.; Conticello, V. P. *J. Am. Chem. Soc.* **2008**, *130*, 49–51. (c) Potekhin, S. A.; Melnik, T. N.; Popov, V.; Lanina, N. F.; Vazina, A. A.; Rigler, P.; Verdini, A. S.; Corradin, G.; Kajava, A. V. *Chem. Biol.* **2001**, *8*, 1025–1032.
23. Ryadnov, M. G.; Woolfson, D. N. *Nat. Mater.* **2003**, *2*, 329–332.
24. Lomander, A.; Hwang, W.; Zhang, S. *Nano Lett.* **2005**, *5*, 1255–1260.

25. (a) Vandermeulen, G. W. M.; Hinderberger, D.; Xu, H.; Sheiko, S. S.; Jeschke, G.; Klok, H.-A. *ChemPhysChem* **2004**, *5*, 488–494. (b) Klok, H.-A.; Vandermeulen, G. W. M.; Nuhn, H.; Ro¨sler, A.; Hamley, I. W.; Castelletto, V.; Xu, H.; Sheiko, S. S. *Faraday Discuss.* **2005**, *128*, 29–41. (c) Pechar, M.; Kopečková, P.; Joss, L.; Kopeček, J. *Macromol. Biosci.* **2002**, *2*, 199–206.
26. (a) The peptide pair has a free energy of unfolding ($\Delta G H_2O$) value of 9.6 kcal mol^{-1}. (b) Lindhout, D. A.; Litowski, J. R.; Mercier, P.; Hodges, R. S.; Sykes, B. D. *Biopolymers* **2004**, *75*, 367–375. The amino acid sequences of K and E are based on those of IAAL K3 and IAAL E3, but each has a terminal glycine residue that was included as a spacer between the peptide and the polymer in the hybrids. See also Figure A4 in the Appendices.
27. Mason, J. M.; Arndt, K. M. *ChemBioChem* **2004**, *5*, 170–176.
28. Crick, F. H. C. *Acta Crystallogr.* **1953**, *6*, 689–697.
29. Zhou, N. E.; Kay, C. M.; Hodges, R. S. *J. Biol. Chem.* **1992**, *267*, 2664–2670.
30. Chen, Y. H.; Yang, J. T.; Chau, K. H. *Biochemistry* **1974**, *13*, 3350–3359.
31. Fields, G. B.; Lauer, J. L.; Dori, Y.; Forns, P.; Yu, Y.-C.; Tirrell, M. *biopolymers* **1998**, *47*, 143–151.
32. It should be noted that the CD spectrum of PS-E/K-PEG is not the average of the spectra of PS-E and K-PEG, as would be observed if the peptide blocks were not interacting. The observed amount of helicity is more than double what would be observed if PS-E remained homocoiled in the presence of K-PEG.
33. Lau, S. Y.; Taneja, A. K.; Hodges, R. S. *J. Biol. Chem.* **1984**, *259*, 13253–13261.
34. Israelachvili, J. N.; Mitchell, D. J.; Ninham, B. W. *J. Chem. Soc., Faraday Trans. 1* **1976**, *72*, 1525–1568.
35. On the basis of a comparison of the DLS and TEM data (Table 3), it is believed that the PEG segments do not contribute to the contrast observed in TEM; therefore, the true aspect ratio would be smaller.
36. The measured D_h of K-PEG (5.4 nm) is only slightly larger than that of K (5.1 nm). Also see ref 25a.
37. See the theoretical model section in the Appendices.
38. Dragan, A. I.; Privalov, P. L. *J. Mol. Biol.* **2002**, *321*, 891–908.
39. Claudy, P.; Lètoffè, J. M.; Camberlain, Y.; Pascault, J. P. *Polym. Bull.* **1983**, *9*, 208–215.
40. (a) Mortensen, K.; Brown, W.; Almdal, K.; Alami, E.; Jada, A. *Langmuir* **1997**, *13*, 3635–3645. PS-PEG with block sizes similar to those used in this study (1000 and 3000 g mol^{-1} for PS and PEG, respectively, compared to 1000 and 3500 g mol^{-1} in PS-E and KPEG) forms spherical micelles in D_2O with no intermicellar interactions in the concentration range used in this study that were detectable by small-angle neutron scattering or static or dynamic light scattering. The micelles were very stable with respect to temperature, showing minimal structural changes (a 5% reduction in core size and a somewhat swollen corona) upon heating from ambient temperature to 95 °C. (b) Brown, G. J.; Richards, R. W.; Heenan, R. K. *Polymer* **2001**, *42*, 7663–7673. Small-angle neutron scattering experiments studying aqueous self-assembly of PS-PEG (M_n = 8500 g mol^{-1}) with a PS weight fraction of 0.15 were found to assemble exclusively into spherical micelles. In contrast, PS-E/K-PEG has a similar PS weight fraction (0.11) and forms rod-like micelles.
41. Zhang, L. F.; Eisenberg, A. *Polym. Adv. Technol.* **1998**, *9*, 677–699.
42. Netz, R. R. *Europhys. Lett.* **1999**, *47*, 391–397.

APPENDICES

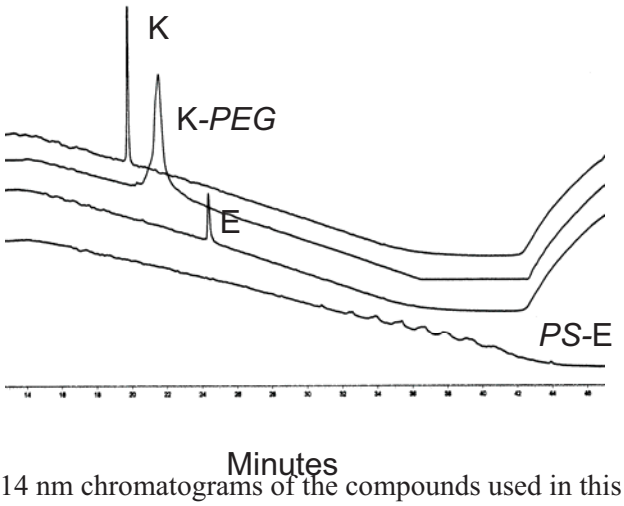

Figure A1. RP-HPLC 214 nm chromatograms of the compounds used in this study.
K, E, and K-PEG: 10% to 90% B over 25 minutes. PS-E: 10% to 100% B over 30 minutes.

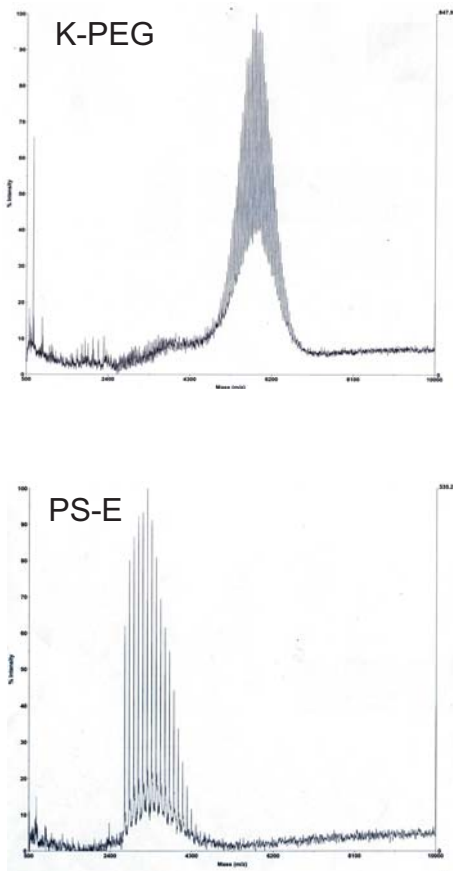

Figure A2. MALDI-TOF mass spectra of the compounds used in this study.

K-PEG

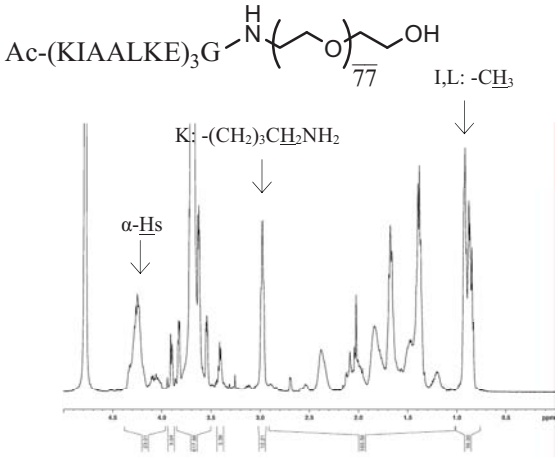

PS-E

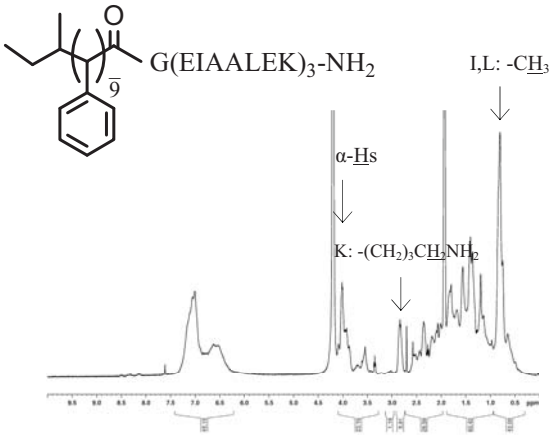

Figure A3. ^{1}H-NMR spectra

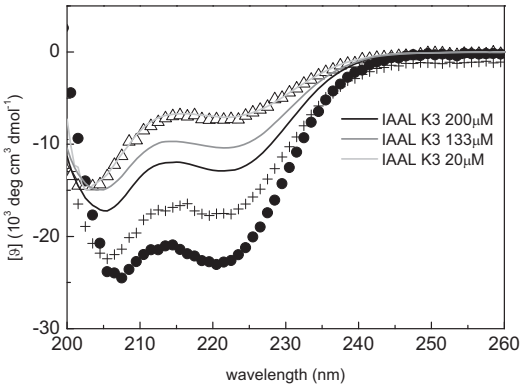

Figure A4. Comparison of K with IAAL K3. CD spectra of K (+), E (Δ), E/K (•) and IAAL K3 that was synthesized for this study (solid lines). [total peptide] = 200 μM unless otherwise stated, PBS, 25˚C.

The amino acid sequence of K was based upon, but is not identical to that of IAAL K3 (Litowski J. R.; Hodges, R. S. *J. Biol. Chem.* **2002**, 40, 37272-37279). K has a C-terminal glycine residue which was included as a spacer between the peptide and polymer in the hybrids. When IAAL K3 was synthesized for this study it had a similar helicity to that reported by Hodges and Litwoski (41% compared to 36%). Interestingly the amount of helicity of IAAL K3 increases with concentration.

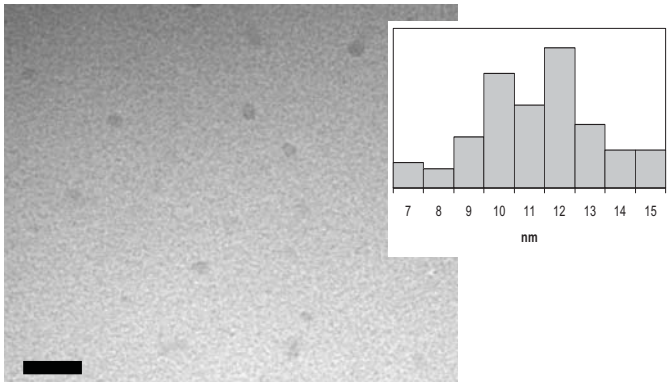

Figure A5. Cryogenic TEM of PS-PEG, with size distribution inset. Scale bar = 50nm. ([PS-PEG] = 440 μM, PBS, 25 °C.) 100 measurements.

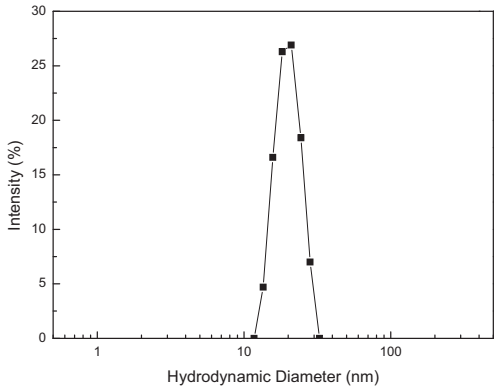

Figure A6. DLS intensity distribution of PS-PEG. ([PS-PEG] = 440 μM, PBS, 25 °C).

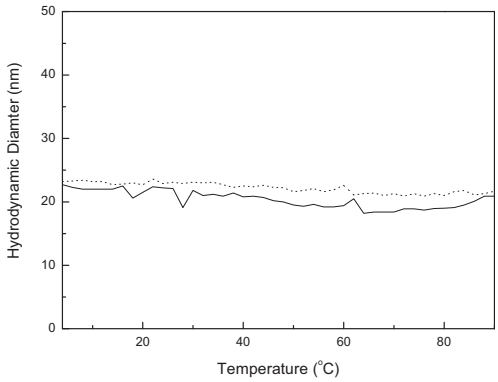

Figure A7. Temperature dependent DLS data for PS-PEG with heating (—) and cooling (····). ([PS-PEG] = 440 μM, PBS, 25 °C).

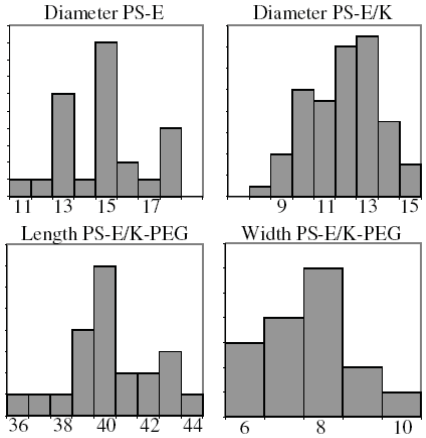

Figure A8. Size distribution of the diameters of PS-E (N=27) and PS-E/K (N=73), and distribution of the lengths (N=22) and widths (N=16) of the worm-like micelles of PS-E/K-PEG. The dimensions are given in nm.

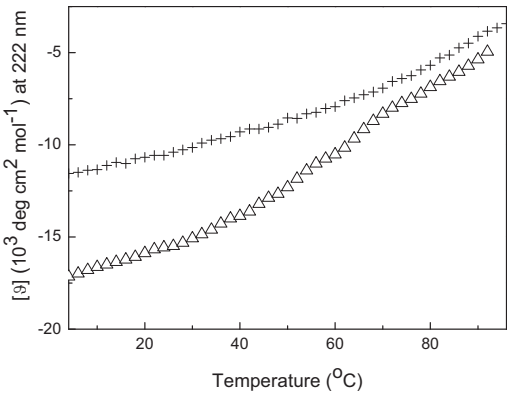

Figure A9. Temperature dependent ellipticity at 222 nm for PS-E (Δ) and PS-E/K (+) recorded at 222nm. ([Total Peptide] = 150-210 μM, PBS).

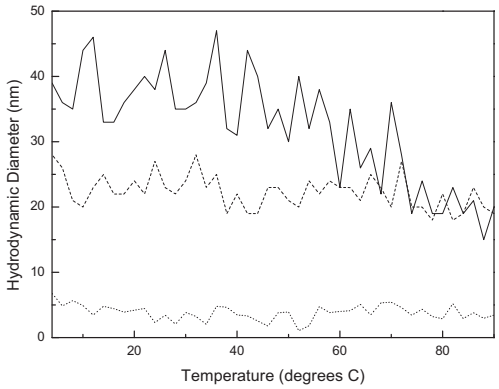

Figure A10. Temperature dependent DLS of PS-E/K-PEG with heating (—), PS-E/K-PEG with cooling (---), and PEG with heating (···). ([Total Peptide] ~ 200 μM, 50 mM PBS).

Theoretical Model

As observed by CD, at about 60 °C the PS-E/K-PEG complex dissociates into PS-E and K-PEG subunits that do not interact with each other. On the micellar scale, at elevated temperature, the rod-like PS-E/K-PEG micelles transform into PS-E spherical micelles suspended in the buffer solution with the K-PEG hybrid. When the solution temperature decreases E/K re-bond, but due to the reduction of solvent in the core and the increase of the surface tension between PS and buffer the PS blocks are no longer mobile and the transition from spherical morphology back to rod-like does not occur.

Being inspired by work of Netz (Netz, R. R. *Europhys. Lett.* **1999**, 47, 391-397.), calculations were made of the free energy of the equilibrium aggregates in the strong segregation limit (Bates, F.S.; Fredrickson, G.H. *Annu. Rev. Phys. Chem.* **1990**, 41, 525-57) when the Flory-Huggins interaction parameter χ has a large value corresponding to no mixing between the PS blocks and peptides/PEG. In this case, the interface between the PS domain and the buffer soluble macromolecules forms, and can be characterized by surface tension defined (Helfand, E.; Tagami, Y. *J Chem. Phys.* **1972**, 56, 3592-3601) as $\gamma=k_BT/a^2(\chi/6)^{1/2}$ where a is the Kuhn length of polystyrene. To simplify the model and to reduce it to the level of di-block copolymer, a few assumptions were made.

First, in all cases only neutral block copolymers are considered. For PS-E and PS-E/K complexes with charged E and K peptides, this assumption is justified by the high concentration of salt in the buffer which may strongly screen inter- and intramolecular electrostatic interactions of E and K peptides.

Second, it is assumed that the second virial coefficient and the statistical properties of E, E/K, and E/K-PEG complexes to be the same and as those of flexible chains. However, for PS-E/K-PEG micelles the neutral PEG block may have a different virial coefficient and conformational free energy compared to those of the peptides, due to the difference in rigidity of the blocks. Using this assumption the model predicts the dimensions of the rod-like and spherical micelles experimentally observed, however a more accurate description of PS-E/K-PEG structures requires treatment of this macromolecule as an ABC triblock copolymer with each block having different physical properties.

Third, with regards to the previous assumptions, the temperature annealing plays a role by reducing the hydrophilic block length (from E/K-PEG to E) and the size of corona in the case of the PS-E/K-PEG sample. The PS core becomes frozen when the temperature is lowered.

For the strong segregation limit, as it was mentioned by Bates and Fredrickson[3], the domain size can be estimated from the balance of the interfacial energy and the chain free energy. The free energy per chain in this case can be written:

$$\frac{F}{k_bT}=\frac{3}{2}\frac{R_s^2}{a_s^{\,2}N_s}+\frac{\upsilon_s f}{2}\frac{N_s^2}{V_s}+\frac{\gamma a_c^{\,3}dN_c}{k_bTR_c}$$

where the first term on the right hand side is the entropic contribution from the corona, the second term is the free energy of the short range interaction between monomers of the corona, and the last contribution comes from the interfacial energy. γ is the interfacial tension between the melt of hydrophobic blocks and the solvent and f is the aggregation number. R_s (s = E, E/K, E/K-PEG or PEG) is the size of the corona, R_c (c = PS) is the size of core, a denotes the Kuhn length, and N_s/N_c is the polymerization index of the corona/core block respectively. υ_s is the second virial coefficient of the hydrophilic block, and

$$V_s = fa^3 N_c \left[\left(\frac{R_s}{R_c} + 1 \right)^d - 1 \right]$$

is the volume of the corona, which depends on the dimension of the secondary structure: d = 1 (lamella), d = 2 (rod), d = 3 (sphere).

Following (Netz, R. R. *Europhys. Lett.* **1999**, 47, 391-397.), two limits are considered when the size of the corona is much larger than the size of core, $R_s/R_c >> 1$, or vice versa, $R_s/R_c << 1$. Under these limits functions can be solved to provide the sizes of the core and corona as well as the minimum free energy of the micellar structure. For the complexes containing PEG the limit of $R_s/R_c >> 1$ was used. Experimentally, for PS-E and PS-E/K complexes the size of the PS core is in the same order of magnitude as the peptide corona, $R_c \approx R_s$. For this reason the micellar properties of PS-E and PS-E/K at both limits are calculated.

After minimization of the free energy over the size of the corona, R_s, and further over the core size, R_c, the size of the core is obtained:

$$R_c = \begin{cases} c_1 \left(\frac{\gamma}{k_B T} \right)^{1/3} a_c a_s^{2/3} N_c^{1/3} N_s^{1/3} \left(\frac{2}{\upsilon_s} \left(\frac{\gamma}{k_B T} \right)^{2/3} a_c^5 a_s^{-2/3} N_c^{5/3} N_s^{-7/3} \right)^{\frac{2}{5}}, & R_s << R_c \\ c_d \left(\frac{\gamma}{k_B T} \right)^{1/3} a_c a_s^{2/3} N_c^{1/3} N_s^{1/3} \left(\frac{2}{\upsilon_s} \left(\frac{\gamma}{k_B T} \right)^{2/3} a_c^5 a_s^{-2/3} N_c^{5/3} N_s^{-7/3} \right)^{\frac{2}{2+3d}}, & R_s >> R_c \end{cases}$$

where c_d are the coefficients of the order of unity. The size of the corona is derived from the first derivation of the free energy with respect to the corona size.

$$R_s = \begin{cases} \left(\frac{1}{6} \frac{\upsilon_s N_s^3 a_s^2 R_c}{d a_c^3 N_c} \right)^{\frac{1}{3}}, & R_s << R_c \\ \left(\frac{d}{6} \frac{\upsilon_s N_s^3 a_s^2 R_c^d}{a_c^3 N_c} \right)^{\frac{1}{2+d}}, & R_s >> R_c \end{cases}$$

The minimal free energy of the aggregate becomes:

$$F/k_bT = \begin{cases} \left(\frac{5}{2}\right)3^{\frac{1}{5}}\left(\frac{\gamma}{k_BT}\right)^{2/3} a_c^2 a_s^{-2/3} N_c^{2/3} N_s^{-1/3} \left(\frac{2}{\upsilon_s}\left(\frac{\gamma}{k_BT}\right)^{2/3} a_c^5 a_s^{-2/3} N_c^{5/3} N_s^{-7/3}\right)^{-\frac{2}{5}}, & R_s << R_c \\ \left(1+\frac{3}{2}d\right)\left(\frac{d}{3}\right)^{-\frac{d}{2+3d}}\left(\frac{\gamma}{k_BT}\right)^{2/3} a_c^2 a_s^{-2/3} N_c^{2/3} N_s^{-1/3} \left(\frac{2}{\upsilon_s}\left(\frac{\gamma}{k_BT}\right)^{2/3} a_c^5 a_s^{-2/3} N_c^{5/3} N_s^{-7/3}\right)^{-\frac{2}{2+3d}}, & R_s >> R_c \end{cases}$$

In the limit of a small corona, $R_s << R_c$, the free energy does not depend on the symmetry of the aggregate: spheres, rods and lamellae have the same free energy. This phase is known as a degenerate phase where all morphologies can be observed at high polymer concentrations at the same time. However, at low polymer concentrations only spheres are formed.

For the opposite limit, $R_s >> R_c$, the rod-like structures are possible when:

$$0.008 < \frac{2}{\upsilon_s}\left(\frac{\gamma}{k_BT}\right)^{2/3} a_c^5 a_s^{-2/3} N_c^{5/3} N_s^{-7/3} < 0.038$$

estimated by equating free energies of different aggregates. PS-E/K-PEG falls within these values. This last equation shows that rods can be assembled by tuning the parameters of the hydrophobic/hydrophilic blocks as well as the interface tension and the interaction between chains within the corona. For PS-PEG, PS-E and PS-E/K the ratio between parameters falls out of the region of rod-like structures and only spherical micelles form.

The rod-like structure of the PS-E/K-PEG aggregates can be changed into spherical micelles by dissociation of the PS-E/K-PEG into PS-E and K-PEG (as observed experimentally at elevated temperature). Upon reassociation of K-PEG with the PS-E spherical micelles there is no transition back to rod-like micelles because the surface tension is too high.

To evaluate the dimensions of the experimentally observed self-assembled structures, the model presented above was used. The number of statistical Kuhn units (Nc, Ns) was chosen to match the model with experimental data and values given in the literature (each statistical unit is equivalent to two monomer units, i.e. two styrene or ethylene glycol units or several amino acids). The Kuhn length was taken to be 0.9-1.15 nm (PS), and 1.05-1.55 nm (PEG, peptides). These numbers are within the reported values for PS and PEG, which lie between 0.5 and 2 nm. The second virial coefficient is unknown for peptides, but the values were chosen to be close to the volume of the monomer. To calculate the interfacial tension for the strong segregation limit, χ = 140. The results of these calculations are presented in the Table A1.

Table A1. Parameters of the molecules, and properties of the micelles that they form as predicted by the model.

Polymer	Limit	a_c [nm]	a_s [nm]	N_c	N_s	V_s [nm^3]	D_c [PS] [nm]	R_s [pept+PEG] [nm]	D [nm]	Morph
PS-E	$R_s >> R_c$	0.9	1.35	4	4	25.70	3.86	4.86	13.6	spheres
PS-E	$R_s << R_c$	0.9	1.35	4	4	0.12	12.34	1.57	15.5	spheres
PS-E/K	$R_s >> R_c$	0.9	1.15	4	4	15.9	3.74	4.47	12.7	spheres
PS-E/K	$R_s << R_c$	0.9	1.35	4	4	0.12	10.54	1.54	13.6	spheres
PS-E/K-PEG	$R_s >> R_c$	0.95	1.05	4	45	0.043	4.20	6.57	17.3	rods
PS-E/K-PEG[1]	$R_s >> R_c$	0.9	1.15	4	45	0.120	3.74	6.97	17.7	spheres
PS-PEG	$R_s >> R_c$	0.95	1.05	5	40	0.850	6.01	7.18	20.4	spheres

The results represented in the Table agree with the experimental findings (Table 3, main text). Although, the model does not take into account the morphology of peptides, it can predict the dimensions of micelles using estimates of the statistical parameters of molecules. The model explains the decrease in size of spherical PS-E micelles when E/K complexation occurs by the decrease of the peptide's rigidity and the decrease in the second virial coefficient (for the $R_s << R_c$ limit). For the opposite limit $R_s >> R_c$ the dimension of spherical micelles is very similar. For rod-like micelles, the end-capping energy should be included in the model, as this may play an important role for short rods close to the transition boundaries. The segregation between peptides and PEG blocks may be considered in more complicated models for the tri-block copolymers where the rigidity of peptides and their structure are known. [1]After annealing PS-E/K-PEG spherical micelles are no longer in equilibrium.